Full-Acoustic Assessment of Digital MEMS Microphones for Traffic Noise Monitoring

María Campo-Valera, Fabio Saba, Mario Corallo, Paolo Guidorzi, Andrea Osele, and Carlo Costa

***Abstract*—Traffic noise is a major environmental pollutant affecting public health and quality of life. Although sound level meters (SLMs) compliant with IEC 61672 and IEC 61260 provide reliable measurements, their high cost limits large-scale deployment. Digital micro-electro-mechanical systems (MEMS) microphones offer a compact and cost-effective alternative for distributed monitoring networks; however, their integrated digital architecture prevents conventional electrical testing, challenging metrological traceability and regulatory compliance. This work presents a full-acoustic verification methodology for digital MEMS microphones intended for sound level metering, inspired by IEC 61672-3. The method uses controlled playback of standardized test tones and representative traffic noise signals in an anechoic test box. Unlike established approaches for conventional SLMs verification based on both electrical and acoustic tests, the proposed methodology introduces a full-acoustic, SI-traceable verification framework tailored to digital MEMS architectures. By leveraging easily controllable pressure-field comparison techniques against a reference microphone, this method guarantees measurement accuracy and reliability while facilitating repeatability. It allows for the consistent characterization of sensitivity, frequency response, and dynamic performance under realistic conditions, resulting in a scalable, metrologically robust, and cost-effective solution for advanced traffic noise monitoring applications.**

***Index Terms*—Acoustic metrology, distributed acoustic sensing, measurement uncertainty, micro-electro-mechanical systems (MEMS) sensor calibration, pressure-field calibration, sound level meter (SLM) verification, traffic noise.**

I. Introduction

TRAFFIC noise represents one of the most pervasive forms of environmental pollution affecting populations worldwide, with profound implications for public health and quality of life [1], [2]. Chronic exposure to elevated noise levels has been linked to a wide spectrum of adverse outcomes, including sleep disturbances, cognitive impairments, cardiovascular diseases, and increased stress levels [3], [4]. As urbanization accelerates globally, the need for precise, continuous, and scalable noise monitoring solutions becomes critical for effective environmental management, regulatory compliance, and informed urban planning [5], [6], [7].

Traditional sound level meters (SLMs), compliant with international standards such as IEC 61672-1 [8], remain the benchmark instruments for environmental noise measurement. These devices provide highly accurate and reliable results through well-established verification procedures. However, their high acquisition and maintenance costs, limited portability, and significant power requirements restrict deployment density, thereby limiting spatial coverage in large-scale noise monitoring campaigns.

In response to these limitations, the emergence of low-cost acoustic sensor networks based on digital micro-electro-mechanical systems (MEMS) microphones has significantly advanced the field of environmental noise monitoring [9], [10], [11], [12], [13]. MEMS microphones offer several advantages: miniaturization, cost efficiency, mechanical robustness, low-power consumption, and integrated digital interfaces, pulse density modulation (PDM) and inter-IC sound (I^2S) [14]. These features make them particularly suitable for large-scale distributed deployments in smart city applications.

Despite these benefits, MEMS-based sensing systems face major challenges in metrological validation and compliance with international standards [15], [16], [17], [18], [19]. Unlike traditional condenser microphones, digital MEMS devices encapsulate both the analog transducer and the analog-to-digital converter (ADC) within a single package, which prevents direct access to the analog signal chain. This architectural integration precludes the application of conventional IEC 61672-3 electrical substitution tests [20], which rely on injecting test signals directly into a microphone-equivalent load adapter. Furthermore, MEMS sensors exhibit inherent variations in noise floor, resonant peaks, and bandwidth limitations [21]. These factors can affect measurement accuracy, particularly at low sound pressure levels or in complex noise environments.

Current calibration methods for MEMS microphones predominantly rely on acoustic comparison and substitution

Received 27 November 2025; revised 9 March 2026; accepted 12 May 2026. Date of publication 4 June 2026; date of current version 12 June 2026. This work was supported by the Autostrada del Brennero S.p.A. in the Framework of the Study of an Acoustic Micro-Electro-Mechanical Systems (MEMS) Sensors Network for Motorway Noise Monitoring. The work of María Campo-Valera was supported in part by MICIU/AEI/10.13039/501100011033 under Grant PID2023-148214OB-C21 and in part by the Fondo Europeo de Desarrollo Regional/European Union (FEDER/EU). The Associate Editor coordinating the review process was Dr. Yixin Ma. *(Corresponding authors: Fabio Saba; María Campo-Valera.)*

María Campo-Valera is with the School of Engineering and Technology, Universidad Internacional de la Rioja (UNIR), 26006 Logroño, Spain (e-mail: mariamercedes.campo@unir.net).

Fabio Saba and Mario Corallo are with the Istituto Nazionale di Ricerca Metrologica (INRiM), 10135 Turin, Italy (e-mail: f.saba@inrim.it; m.corallo@inrim.it).

Paolo Guidorzi is with the Department of Industrial Engineering (DIN), Università di Bologna, 40126 Bologna, Italy (e-mail: paolo.guidorzi@unibo.it).

Andrea Osele and Carlo Costa are with Autostrada del Brennero S.p.A., 38121 Trento, Italy (e-mail: andrea.osele@autobrennero.it; direzione.tecnica.generale@autobrennero.it).

Digital Object Identifier 10.1109/TIM.2026.3699785

TABLE I
COMPARISON OF RELATED WORKS ON MEMS MICROPHONE CALIBRATION AND SYSTEM VERIFICATION APPROACHES

Reference	Target application	MEMS type	Calibration method	SLM assessment	Realistic noise test	Approach
Mydlarz *et al.* [9]	Urban noise monitoring networks	Analog	Free-field comparison	Yes	Yes	SLM system assessment by simultaneous comparison against a class 1 SLM in an anechoic chamber
Mello *et al.* [11]	Autonomous noise monitoring system	Digital	Free-field comparison and low frequency pressure cavity	No	Yes	Frequency response determination and digital correction filter implementation
Mello *et al.* [13]	Embedded noise monitoring system	Digital	Not specified	Yes	Yes	Design embedded system focusing on SLM algorithm
Chan *et al.* [16]	MEMS microphone bulk calibration	Not specified	Diffuse-field comparison	No	No	Simultaneous calibration of several MEMS microphones in the reverberation chamber
Prato *et al.* [19]	MEMS microphone calibration	Digital	Pressure-comparison implemented in hemi-anechoic chamber	No	No	Metrological characterization of digital MEMS microphone sensitivity and uncertainty analysis
Saba *et al.* [23]	MEMS microphone calibration	Analog	Pressure-comparison in closed active coupler	No	No	Analysis of acoustic field non-uniformities in comparison couplers and their compensation
This work	**Traffic noise monitoring**	**Digital**	**Pressure-comparison implemented in anechoic test box**	**Yes**	**Yes**	**Full-acoustic SLM evaluation with digital format compatibility and comparison to a laboratory standard microphone**

techniques using pure tones or broadband signals under laboratory conditions [15], [19]. While useful for baseline validation, such methods are not comprehensive enough to provide a complete assessment of the capability to capture the highly dynamic and spectrally complex characteristics of traffic noise, which includes broad frequency content, transient events, and fluctuating levels [9], [22]. Moreover, the lack of standardized procedures specifically designed for digital MEMS microphones limits regulatory acceptance and hinders their integration into official monitoring networks.

This work addresses these limitations by introducing a comprehensive full-acoustic verification methodology for digital MEMS microphones, which is tailored for sound level metering and inspired by the framework of IEC 61672-3, but designed to circumvent the restriction of electrical tests. The proposed approach employs controlled playback of both standardized test waveforms and representative traffic noise signals inside an anechoic test box, enabling repeatable and traceable acoustic characterization. These test signals incorporate realistic spectral and temporal features of common traffic noise sources, such as conventional vehicle traffic, motorway construction machinery, and two-stroke engine operation, ensuring high relevance to practical monitoring scenarios.

This full-acoustic procedure provides a scalable and cost-effective alternative to conventional calibration setups, ensuring traceability and reproducibility. In this context, the main contribution of this article lies in the definition of a full-acoustic, traceable verification methodology for digital MEMS microphones, which overcomes the intrinsic limitations of electrical testing and expands the scope of conventional acoustic characterization. By incorporating standardized test signals and realistic traffic noise scenarios, the methodology ensures measurement reliability and traceability through simultaneous comparison against a reference microphone under easily controllable pressure-field conditions, which are not subject to the diffraction phenomena occurring in free-field conditions. Furthermore, this full-acoustic approach enables an end-to-end assessment of the influence of the microcontroller-provided clock on measurement accuracy, specifically regarding jitter-induced errors in the ADC. Table I compares related works in terms of calibration methodology and system verification approach.

The article is organized as follows. In Section II, a modular and traceable measurement architecture is introduced, consisting of four stages that enable the acoustic characterization of a digital MEMS microphone. Section III describes the measurement system employed to achieve traceable acoustic calibration. Section IV presents the metrological characterization of the system, covering both electrical and acoustic evaluations to determine the overall gain and microphone sensitivity, respectively. Finally, once the system is fully characterized, Section V applies two case studies to assess the

performance of the MEMS microphone: the first focuses on experimental evaluation following standardized criteria, while the second addresses validation under representative traffic noise scenarios. Finally, in Section VI, we point out concluding remarks.

II. Architecture

This work relies on a modular and traceable architecture that enables the controlled acoustic characterization of an I^2S (Inter-IC Sound) digital MEMS microphone (hereafter referred to as mic_{test}) integrated with a high-performance microcontroller. This is compared with a calibrated Laboratory Standard (LS) microphone (denoted as mic_{ref}). Such a modular architecture enables the deliberate isolation and validation of each subsystem of the measurement chain.

While the microcontroller can operate as a digital acquisition system (DAQ) natively via the I^2S protocol, paving the way for a fully integrated, standalone sound level meter, the initial stage of development allows for the metrological validation of the MEMS sensor's output independently. Currently, the microcontroller functions as a clock and power supply unit in this architecture, enabling the digital audio stream to be extracted cleanly and without interference.

MEMS microphones with an I^2S interface were chosen instead of those with a PDM interface, given the presence of the ADC converter and anti-aliasing filter on board, implemented by the manufacturer. This way, the digital signal output from the microphone does not require external processing and filtering, which could be implemented by the user in a nonunivocal way, leading to different and possibly even incorrect results.

The architecture consists of four main stages.

1) *Generation of the Acoustic Field*: A loudspeaker generates a controlled sound field inside an anechoic test box, with the mic_{ref} providing reference measurements of sound pressure. This ensures metrological traceability and enables consistent playback of test signals and traffic noise spectra with high repeatability.
2) *Acoustic signal transduction*: The digital MEMS microphone is exposed to the same acoustic field simultaneously with the mic_{ref}. The mic_{test} integrates on-chip ADC and outputs PCM audio via I^2S, with a microcontroller providing the required, bit clock (BCLK/SCK) and channel select (LRCLK/WS) signals, and also power supply. This configuration constitutes the device under test (DUT).
3) *Digital-to-Analog Conversion for DAQ Compatibility*: Since the MEMS microphone outputs a fully digital signal, an external digital-to-analog converter (DAC) is employed to convert the digital data into an analog signal, enabling the connection to the reference laboratory-grade sound analyzer, which operates with analog voltage inputs. This stage ensures the preservation of spectral fidelity and dynamic range, enabling seamless integration with traceable analog instrumentation.
4) *Signal Analysis and Postprocessing*: The analog output from the DAC is fed into a high-precision spectrum analyzer, which is connected to a PC software suite. This setup functions as a metrologically traceable DAQ system, enabling the computation of standardized acoustic metrics such as L_{eq}, third-octave band levels, and other relevant environmental noise indicators.

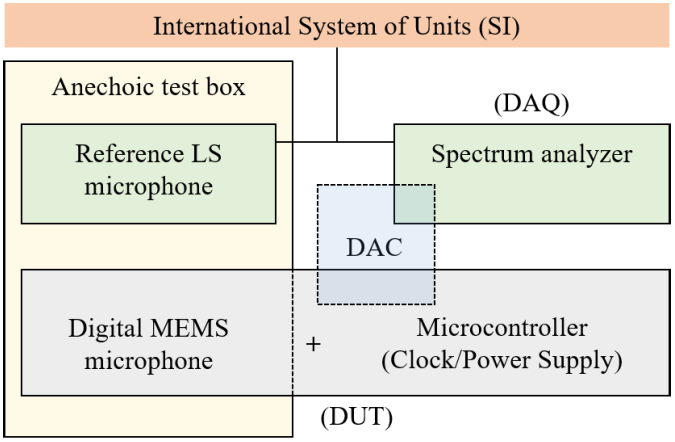

Fig. 1. Schematic of the measurement system for SI-traceable acoustic characterization of digital MEMS microphones.

This modular architecture provides a robust framework for benchmarking MEMS microphones against reference equipment and maintains compatibility with conventional acoustic analysis methods. It also paves the way for fully integrated, microcontroller-based SLMs, which support the development of scalable, low-cost sensor networks for traffic noise monitoring.

III. Measurement System

A dedicated measurement system was developed to assess the acoustic performance of the digital MEMS microphone in traffic noise monitoring applications and enable metrologically traceable acoustic characterization. The system comprises three main components: 1) the device under test (DUT); 2) a digital-to-analog converter (DAC); and 3) reference standard instrumentation traceable to the international system of units (SI). This includes an LS microphone and a spectrum analyzer (DAQ). Measurements were conducted inside the Brüel and Kjær Type 4232 anechoic test box [24], and the overall measurement schematic, including the traceability path to the SI, is illustrated in Fig. 1. A summary of the instruments used can be found in Appendix A.

A. Digital Mems Microphone and Microcontroller

The device under test (DUT) is composed of the Adafruit I^2S MEMS Microphone Breakout evaluation board, which is built around the Knowles SPH0645LM4H-B sensor [25]. This bottom-port digital microphone integrates on-chip analog-to-digital conversion and delivers audio data via I^2S output. The microphone features a flat frequency response (50 Hz to 15 kHz), -26 dBFS $\pm$ 3 dB digital sensitivity, and 65 dB SNR. It supports SPLs up to 120–130 dB. Its compact size and omnidirectional directivity make it ideal for embedded environmental noise monitoring applications [26].

The microphone interfaces with a Teensy 4.1 microcontroller [27], which is equipped with a 600 MHz ARM Cortex-M7 core and native I^2S support. The measurement setup used in this work was set to a sampling frequency of 44.1 kHz and 16-bit audio data, for the widest compatibility with different types of MEMS microphones. The Teensy platform has sufficient memory and computational power for real-time spectral analysis [10] and 24-bit audio data multichannel sampling at higher sampling frequencies, as well as the possibility of data storage and addition of wireless communication modules for possible integration into a future network.

The digital MEMS microphone and the microcontroller together form the DUT, which balances performance, energy efficiency, and cost-effectiveness, making it a promising platform for scalable, next-generation acoustic sensing.

B. Digital-to-Analog Converter

The digital-to-analog conversion board (DAC) implements a Texas Instruments PCM5102A chip [28], which supports I^2S connection and is capable of sampling rates up to 192 kHz and 24-bit audio data, with a nominal dynamic range exceeding 112 dB. It should be noted that the DAC board is required only for the laboratory assessment procedure of the MEMS microphone described in this article, while the implementation of the system in a low-cost device does not require this circuit part.

Including and characterizing a DAC in the measurement chain establishes a practical and reproducible procedure for conducting full-acoustic assessments of digital MEMS microphones under controlled laboratory conditions. This provides a reliable framework for consistent evaluation and benchmarking.

C. Reference Microphone and Spectrum Analyzer

Two high-precision reference instruments are employed for metrological validation. First, the Brüel and Kjær Type 4180 LS2 microphone [29] is used as the reference microphone. This 1/2-inch laboratory standard condenser microphone has a flat frequency response up to 20 kHz, high sensitivity, and extremely low self-noise. It complies with IEC 61094-1 [30] standard and is widely recognized for its accuracy and stability in traceable acoustic measurements. Second, the Ono Sokki DS-3200 Multichannel Data Station spectrum analyzer [31], integrated with a PC-based software suite, is used for real-time acoustic signal analysis (DAQ). It supports third-octave band processing, offers a wide dynamic range, and conforms to the specifications of IEC 61672-1 [8] and IEC 61260-1 [32]. In the proposed setup, the DS-3200 processes the analog output from the DAC to compute standardized acoustic metrics, such as the equivalent continuous sound pressure level L_{eq}, providing a reliable reference for assessing the performance of the digital MEMS microphone.

IV. Metrological Characterization

The metrological characterization of the proposed measurement system includes a comprehensive calibration procedure and a structured uncertainty analysis. This section details both the electrical and acoustic calibration stages required to establish traceability to the International System of Units (SI), as well as the identification and quantification of the main uncertainty contributions affecting the MEMS microphone response. The procedure is structured into two phases: 1) the electrical characterization of the entire acquisition chain, excluding the microphones and 2) the acoustic characterization of the microphones, including the determination of the sensitivities of both the mic_{test} and the mic_{ref}.

The first phase evaluates the electrical characteristics of the entire system, including the total gain introduced by the preamplifier and connection cables. To isolate and quantify electrical noise and transmission losses that could affect the reliability of the acquired data, comparative measurements were performed both including and excluding gain contributions, such as those from the microphone's cabling within the anechoic test box. Additionally, since the DAC is a critical element of the measurement chain, its key performance characteristics were verified.

The second phase determines the sensitivity of the mic_{test} by comparing it with the mic_{ref}, whose sensitivity is preliminarily determined by primary reciprocity calibration. This establishes the metrological traceability of the mic_{test} measurements. Numerical simulations are used to correct for acoustic pressure nonuniformities that occur during the pressure-comparison calibration of the mic_{test} inside the anechoic test box.

A. Electrical Characterization

Reference Signal Chain: The electrical characterization quantifies the contributions of gains G in dB introduced by components in the reference signal acquisition chain, defined as $G = 20\log_{10}(V_{out}/V_{in})$, where V_{out} and V_{in} are the output and input voltages of the respective components in the signal acquisition chain. This process isolates the acoustic response of the mic_{ref} from the electrical characteristics resulting from the amplification stages, impedance mismatches, and interconnections.

The signal path in the reference chain includes the following.

1) G_{pre}: the gain of the Brüel and Kjær Type 2673 [33] insert voltage preamplifier, which is connected to the mic_{ref} through the anechoic test box extension cable,
2) G_{ad}: the gain associated with the Brüel and Kjær Type JJ 2615 load adapter (a capacitive matching circuit of 18 pF to replicate the microphone's capacitive load),
3) G_{cable}: the gain due to the extension cable of the anechoic test box, which connects the mic_{ref} with the insert voltage preamplifier.

Two measurement phases were performed to identify and quantify each contribution: 1) measurements without the extension cable of the anechoic test box: this allowed us to discriminate the gain of the insert voltage preamplifier and the gain of the load adapter and 2) measurements with the extension cable of the anechoic test box: this allowed us to determine the overall gain of the system, G_{box}, which includes

the gain of the load adapter, extension cable interconnection, and insert voltage preamplifier.

Appendix B provides detailed connection diagrams for the respective measurement phases.

Fig. 2 presents the experimental setup used to measure the gains of the insert voltage preamplifier and load adapter.

1) *Measurements Without the Extension Cable of the Anechoic Box:* When the insert voltage preamplifier is connected in series with the load adapter, the combined gain, $G_{\text{pre+ad}}$, is measured by injecting the signal into the load adapter input. It can be expressed as follows:

$$G_{\text{pre+ad}} = G_{\text{pre}} + G_{\text{ad}}. \tag{1}$$

When the signal is injected into the insert voltage input of the preamplifier, the load adapter, which is connected in series with the preamplifier, is bypassed, and the gain, G_{pre}, is measured directly.

2) *Measurements With the Extension Cable of the Anechoic Box:* When the load adapter is connected to the insert voltage preamplifier via the anechoic test box extension cable, the system's overall gain, denoted by G_{box}, is measured by injecting the signal into the load adapter input. The measurement can be expressed as follows:

$$G_{\text{box}} = G_{\text{pre}} + G_{\text{ad}} + G_{\text{cable}}. \tag{2}$$

These experimental measurements allow us to infer the gain introduced solely by the extension cable using (1) and (2) as:

$$G_{\text{cable}} = G_{\text{box}} - G_{\text{pre+ad}}. \tag{3}$$

Finally, the total external gain, G_{ext}, is defined as the sum of the contributions of the insert voltage preamplifier and extension cable contributions and is expressed as follows:

$$G_{\text{ext}} = G_{\text{pre}} + G_{\text{cable}}. \tag{4}$$

The external gain is a critical correction parameter that must be applied to the measured SPL to ensure the sensitivity analysis of the MEMS microphone reflects its intrinsic acoustic properties. Systematically accounting for these nonacoustic components makes it possible to evaluate the microphone's performance and reduce uncertainties in the calibration process.

As shown in Fig. 3, the gain values of the various components in the reference measurement chain are presented in the frequency range from 100 Hz to 10 kHz. The gain characterization reveals a noteworthy contribution from the extension cable of the anechoic test box, which exhibits increasing attenuation from 2 kHz to 10 kHz.

Test Signal Chain: The electrical characterization of the test signal acquisition chain focuses on assessing the influence of the DAC on the measurements performed with the mic_{test}.

The DAC board used in the measurement system is connected to the Teensy 4.1 microcontroller shown in Fig. 4a; the DAC consists of a low-cost PCM5102A breakout board, which includes a few voltage regulators, power and I^2S communication pins, and two analog audio outputs (left and right channels), as shown in Fig. 4b.

Two types of test signals were generated and delivered to the DAC board using the Teensy platform: 1) white noise at

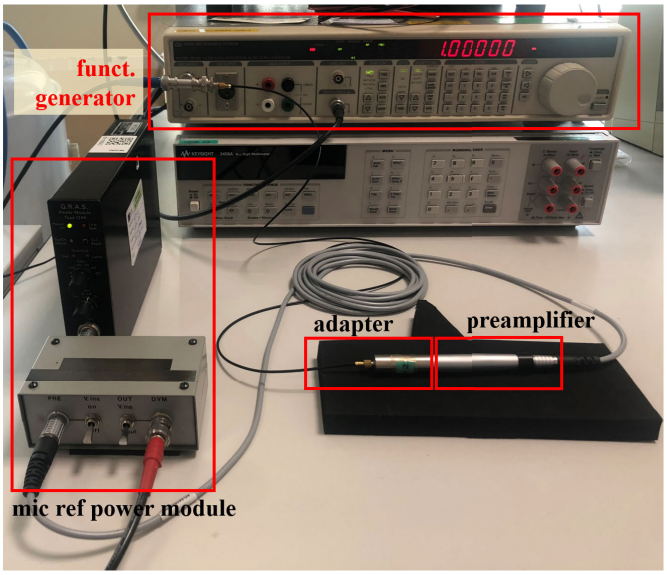

Fig. 2. Experimental setup for the electrical characterization of the insert voltage preamplifier and load adapter gains.

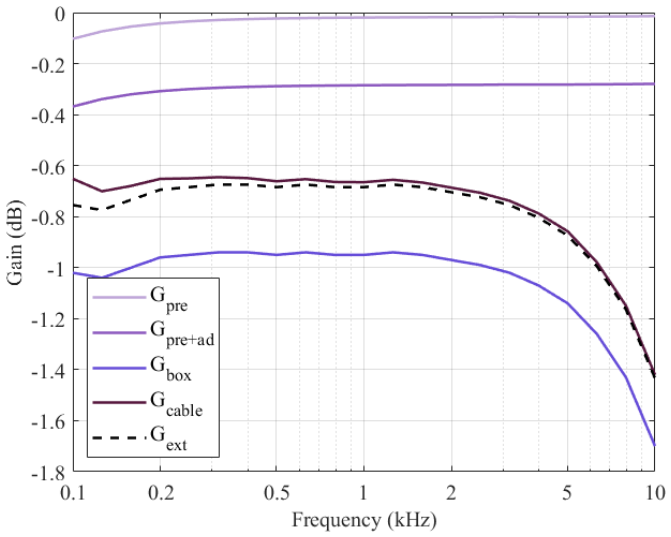

Fig. 3. Measured gain values of the different components in the mic_{ref} measurement chain (solid lines), along with the resulting external gain, G_{ext} (dashed line), plotted as a function of frequency from 100 Hz to 10 kHz.

100 %, 50 %, and 10 % of full scale and 2) pure tones at 100 Hz, 1 kHz, and 10 kHz, all of which were reproduced at the same amplitude levels. One of the DAC board's analog outputs was connected to the Ono Sokki DS-3200 Multichannel Data Station to perform spectral analysis. Additionally, the inherent background noise of the DAC board was characterized under no-signal conditions.

Fig. 5 shows the response of the DAC board when excited by a white noise signal. Since the results are expressed in third-octave bands, a 3 dB/octave weighting filter was applied to the measured data to achieve a flat spectral representation. The uncertainty contribution due to the frequency response of the DAC can be evaluated from the standard deviation of the DAC's output under white noise excitation. Fig. 6 illustrates the deviation of the output levels across the third-octave bands,

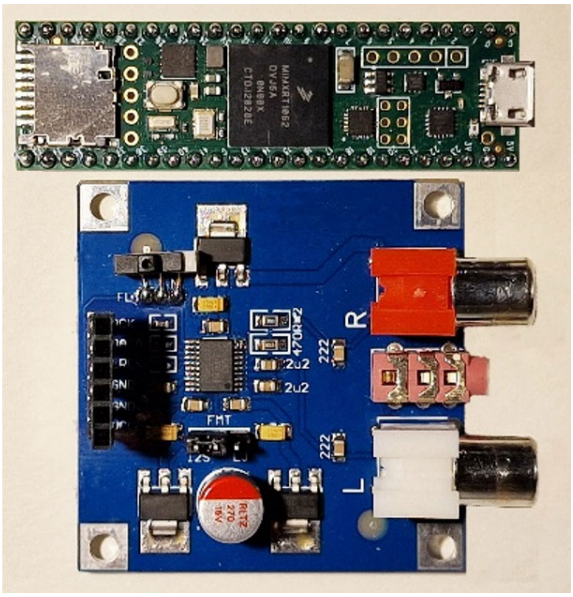

Fig. 4. Hardware components used in the system. (a) Teensy 4.1 microcontroller board. (b) Low-cost PCM5102A DAC board.

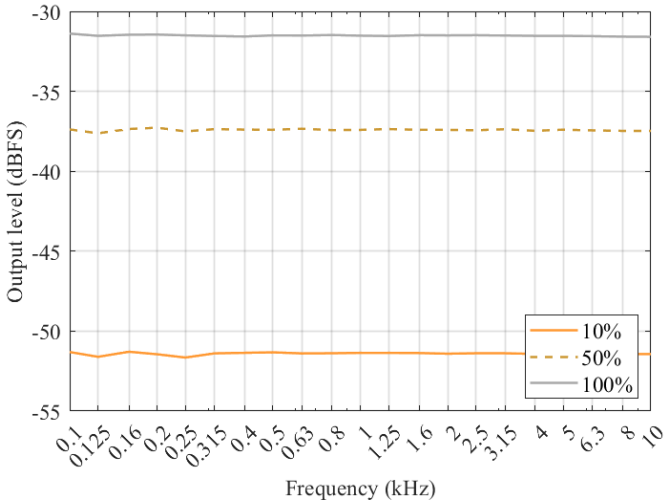

Fig. 5. DAC response to white noise excitation. Measured output in dBFS at three different amplitude levels (expressed as percentages of full scale).

from 100 Hz to 10 kHz, with respect to the reference output level at 1 kHz, for the DAC's response to the white noise excitation. A widening range of deviations can be observed for frequencies below 315 Hz, at lower amplitude levels.

Fig. 7 demonstrates the DAC's amplitude linearity at 100 Hz, 1 kHz, and 10 kHz. This was evaluated using the root mean square error (RMSE) of the fit curves. The low RMSE values confirm the DAC's ability to reproduce signal levels with high fidelity, ensuring accurate signal conversion for rigorous experimental applications.

At no-signal conditions, the inherent background noise measured at the DAC output was less than −126.5 dBFS. Total distortion plus noise (TD + N) values, shown in Table II, were measured by generating the above-mentioned pure tones at different frequencies and amplitudes. Given the amplitude levels of the pure tones and the measured inherent noise

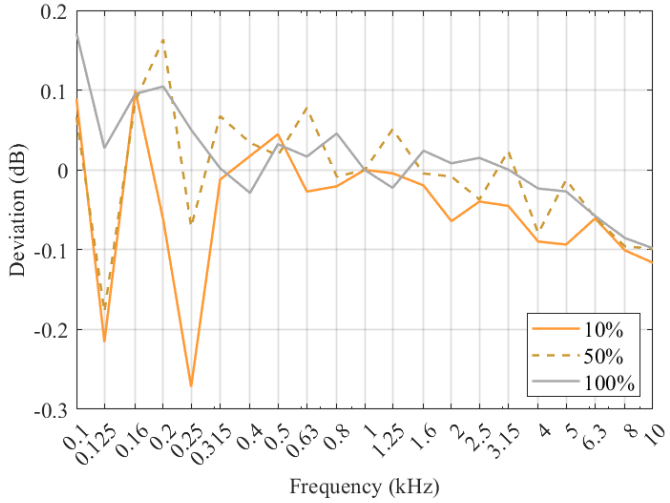

Fig. 6. Deviation of the output levels across the third-octave frequency bands, from 100 Hz to 10 kHz, relative to the 1 kHz reference output level, for the three amplitude levels (expressed as percentages of full scale).

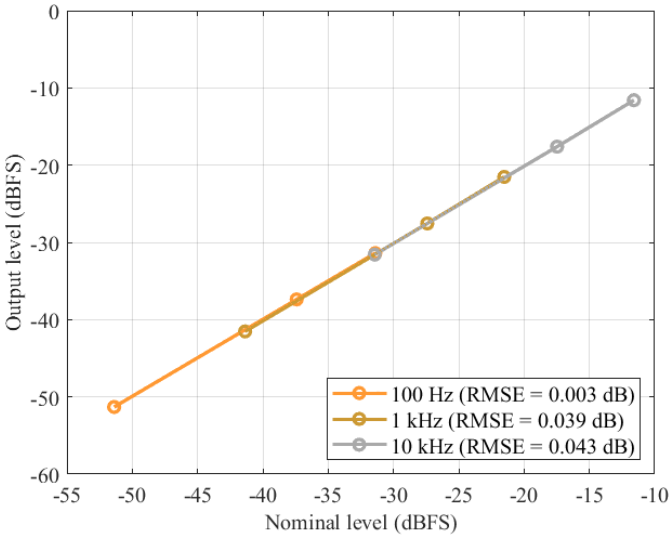

Fig. 7. Amplitude linearity of the DAC at 100 Hz, 1 kHz, and 10 kHz.

TABLE II

TD + N OF THE DAC BOARD, EXPRESSED AS PERCENTAGE, FOR THE THREE AMPLITUDE LEVELS (AS PERCENTAGES OF FULL SCALE) OF THE INPUT SINUSOIDAL SIGNALS AT 100 Hz, 1 kHz, AND 10 kHz

% full scale	100 Hz	1 kHz	10 kHz
10 %	0.06 %	0.05 %	0.03 %
50 %	0.06 %	0.05 %	0.02 %
100 %	0.06 %	0.05 %	0.02 %

floor of the DAC, a residual distortion of less than 10 ppm was evaluated as the main contribution to the measurement uncertainty associated with the distortion.

B. Acoustic Characterization

The sensitivity of the mic_{test} was characterized using the pressure-field comparison calibration method with simultaneous acoustic excitation, as outlined in the cited study [23]. This

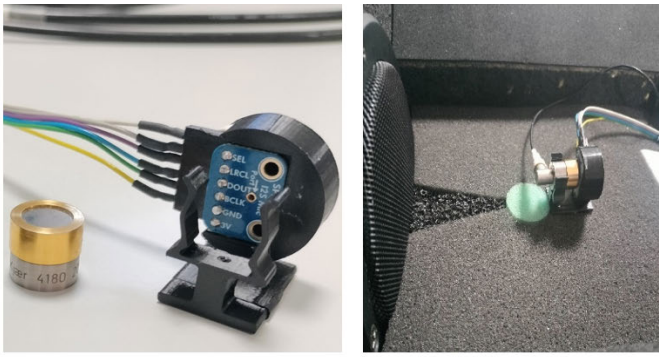

(a) (b)

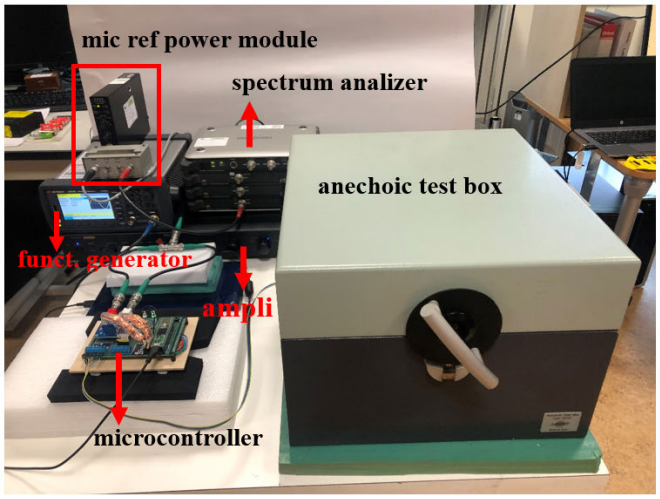

(c)

Fig. 8. Experimental setup of the proposed measurement system. (a) Photograph showing the mic_{ref} (Brüel and Kjær Type 4180 LS2, left) and the mic_{test} (Knowles SPH0645LM4H-B MEMS mounted on the Adafruit I^{2}S MEMS Microphone Breakout, right), placed in a custom 3D-printed support. (b) Both microphones were positioned with their diaphragms aligned coaxially and oriented perpendicularly to the acoustic wavefront generated inside the anechoic test box. (c) Complete experimental setup used for the measurements.

method relies on the precalibrated sensitivity of the mic_{ref}, which was determined using the primary pressure reciprocity method. This ensures that all measurements are traceable to the SI.

The quantity under consideration is the acoustic pressure sensitivity level of the mic_{test}, i.e., the ratio between the output voltage V_{out} of the microphone and the acoustic pressure P, expressed in dB relative to a reference sensitivity of 1 V/Pa [22]:

$$S_{mic,test} = 20\log_{10}\left(\frac{V_{out}}{P}\right). \tag{5}$$

The sensitivity value encompasses the entire signal path, which comprises the Knowles SPH0645LM4H-B MEMS microphone, mounted on its Adafruit I^{2}S evaluation board, connected to the Teensy 4.1 microcontroller [10] with the PCM5102A DAC module.

The implementation of this method entailed the development of customized 3-D-printed microphone holders, which were designed to ensure precise and reproducible positioning. As depicted in Fig. 8a, the MEMS microphone on the right

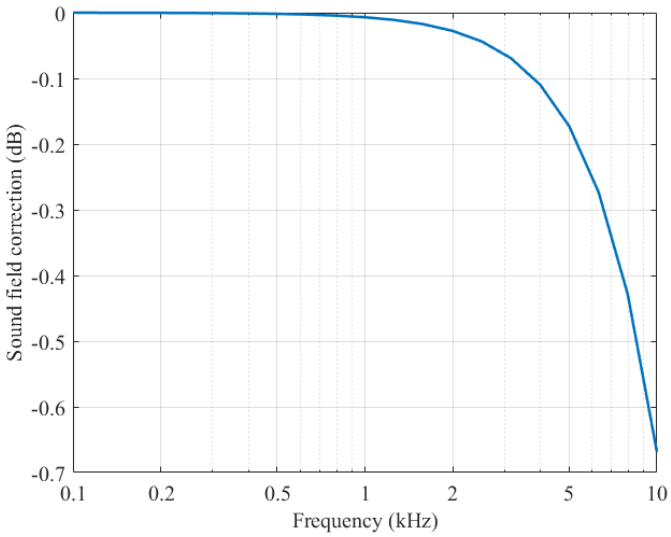

Fig. 9. Sound field corrections obtained from the FEM simulation for the pressure-comparison calibration of the MEMS microphone, mounted together with the reference LS2 microphone in the custom 3-D-printed support.

is integrated into a bespoke 3-D-printed mount, while the mic_{ref} on the left is fastened to the same mount by an elastic hook, with both microphones' diaphragms aligned coaxially. As illustrated in Fig. 8b, the perpendicular orientation relative to the acoustic wavefront generated inside the Brüel and Kjær Type 4232 anechoic test box is evident. To ensure consistent acoustic pressure field conditions across the frequency range, a spacing of less than 2 mm was maintained between microphones. The complete configuration is illustrated in Fig. 8c.

The sensitivity of the mic_{test} was evaluated at third-octave center frequencies from 100 Hz to 10 kHz. To circumvent systematic errors associated with band-averaging methods, FFT analysis was employed, as these methods are sensitive to differences in the frequency responses of MEMS and reference microphones [34].

In particular, the comparison calibration method relies on sensitivity values of the mic_{ref} obtained via primary reciprocity calibration at the exact third-octave center frequencies. Using band-averaging techniques to process the output voltages of the reference and test microphones can therefore introduce errors, especially when their frequency responses differ significantly in slope or shape, a common occurrence between MEMS and conventional LS condenser microphones. FFT analysis of the output signals ensures accurate sensitivity estimation, provided that the acoustic excitation achieves a sufficiently high SNR.

To this purpose, both microphones were simultaneously excited in the anechoic test box with sinusoidal signals, producing SPLs above 90 dB across the entire frequency range. However, given the disparity in dimensions between the mic_{test} acoustic port and the mic_{ref} diaphragm, the occurrence of pressure field nonuniformities is a probable outcome, with the potential to induce calibration errors, particularly at high frequencies [23], [34].

To address this, finite element method (FEM) simulations were performed under an axisymmetric approximation to

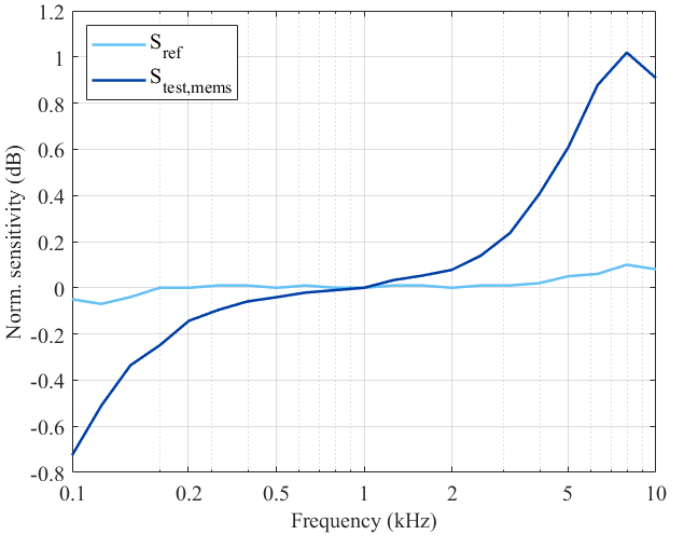

Fig. 10. Sensitivity curves, S_{ref} and $S_{test,mems}$, corresponding to the mic_{ref} and mic_{test} measurement chains, respectively, normalized to their response at 1 kHz.

model the pressure distribution between microphones. The results of the study indicated significant deviations from uniformity above 4 kHz. Consequently, sound field correction factors were derived to address these deviations. As illustrated in Fig. 9, the correction values are plotted as a function of frequency. A more thorough examination of this topic is given by [23].

Notwithstanding the idealized simulation, real-world deviations may still arise from chamber reflections, loudspeaker diffraction, and minor misalignments. Consequently, correction factors were conservatively treated as uniformly distributed between zero (ideal spatially uniform field) and the FEM predicted values.

As illustrated in Fig. 10, the normalized sensitivities of the mic_{test} are presented relative to the sensitivity value at 1 kHz, along with the normalized sensitivity of the mic_{ref}. The latter is obtained by combining the microphone's open-circuit sensitivity with the measured external gain G_{ext}, resulting in a flat frequency response. Conversely, the mic_{test} demonstrates a conspicuous resonance near 8 kHz, a characteristic that is commonly observed in MEMS microphones due to the inherent design of their internal cavity and diaphragm architecture, which is typically fabricated through CMOS-MEMS processes [35].

This marked increase in sensitivity above 4 kHz, along with a significant low-frequency roll-off below 125 Hz, must be considered for the accurate capture of high- and low-frequency sound components. Specifically, the mic_{test} sensitivity curve, derived from the comparison calibration, constitutes a foundational outcome for the effective design and implementation of a correction filter within the microcontroller. This enables the accurate spectral representation of sounds. However, the development of a correction filter is beyond the scope of the present work. The objective of this study is to investigate the performance of the mic_{test} over the characteristic spectral components of the traffic noise, whose energy is typically concentrated in a frequency range where the digital MEMS microphones exhibit a relatively flat response.

The mic_{test} demonstrates adequate sensitivity, and when combined with the robustness, low power, and cost-effectiveness of MEMS technology, it is suitable for large-scale deployment in distributed acoustic sensing networks for traffic noise monitoring.

V. Case Studies

After acoustic and electrical calibration, two case studies were conducted to evaluate the MEMS microphone response: 1) an experimental evaluation according to standardized criteria and 2) an experimental validation in scenarios with traffic noise sources.

The results are reported as measured deviations with respect to the mic_{ref} response, along with their associated uncertainties. The overall uncertainty budget, including a description of the main contributions, is summarized in Appendix C.

The experiments were conducted under the following controlled environmental conditions: static pressure of (98.326 $\pm$ 0.632)kPa, temperature of (23.8 $\pm$ 1.9)°C, and relative humidity of (56.3 $\pm$ 5.5)%.

The experimental setup matches that used for acoustic characterization. A detailed schematic of the setup is shown in Fig. 11.

These two experimental campaigns, one based on standardized test signals and the other on realistic reproductions of environmental noise spectra, provided a comprehensive framework for validating the MEMS-based measurement system in both controlled laboratory conditions and acoustically representative scenarios.

A. Experimental Evaluation Under Standardized Criteria

Inspired by the periodic verification procedures for sound level meters described in the international standard IEC 61672-3 [20], the performance of the mic_{test} was evaluated. The evaluation focused on the mic_{test} response to short-duration acoustic signals and its amplitude linearity. The latter refers to the consistency of the mic_{test} output level in proportion to varying input sound pressure levels across a defined dynamic range. Unlike the standard methodology, which involves injecting electrical test signals into the measurement system via an equivalent load that replaces the microphone, this study employs a fully acoustic testing approach.

There are two motivations for adopting this kind of approach: 1) to evaluate the capability of MEMS microphones to accurately capture and preserve signal fidelity and 2) to avoid the complexity of developing a dedicated electronic interface for electrical testing, which is particularly challenging for digital MEMS microphones. These devices often exhibit significant variability in output protocols, power supply requirements, and clock configurations, which makes designing universal analog test circuits nontrivial. In this context, a controlled acoustic environment, combined with a reference microphone for comparison, provides a reliable and practical alternative.

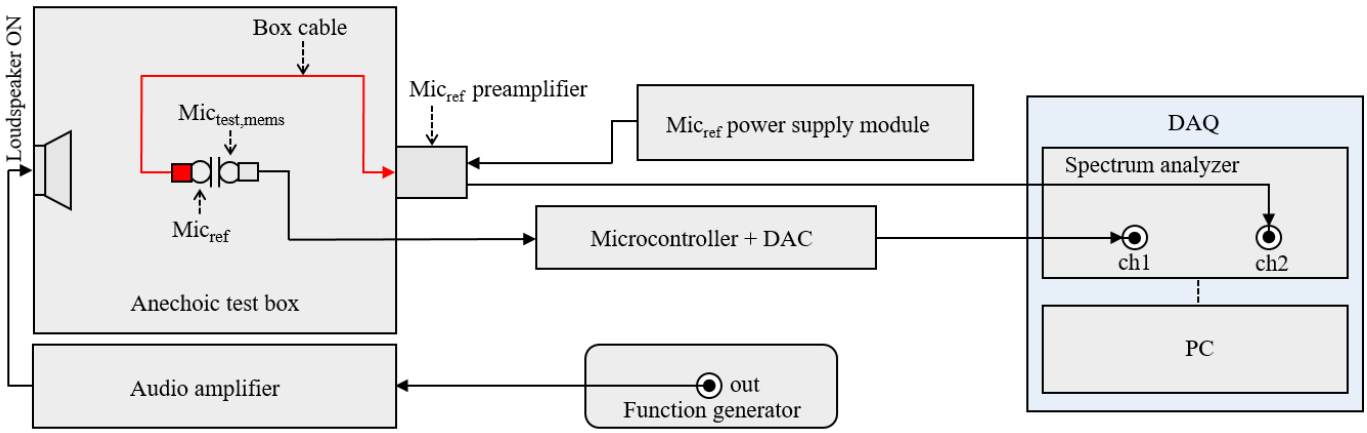

Fig. 11. Schematic of the experimental setup used for the measurements. Test signals are generated by a function generator and delivered to the loudspeaker inside the anechoic test box via an audio amplifier. The output signals from mic_{ref} and $\text{mic}_{\text{test, MEMS}}$ are routed through the insert-voltage preamplifier and the microcontroller with DAC, respectively, to a multichannel spectrum analyzer (DAQ). The mic_{ref} power supply module provides the polarization voltage and power to the reference microphone and its preamplifier, which are connected via the box extension cable.

Tone-burst and linearity tests were performed by acoustically exciting a loudspeaker inside the anechoic test box with controlled signals while simultaneously recording the responses of both the mic_{test} and the mic_{ref}. The microphone arrangement replicated the setup used for the acoustic pressure-comparison calibration.

The sensitivity of the mic_{test} at 1 kHz, determined by the acoustic calibration procedure (see Section IV-B), was used to configure the input channel sensitivity of the spectrum analyzer operating in SLM mode. Similarly, the sensitivity of the mic_{ref} at 1 kHz was used to configure the corresponding analyzer input channel. This ensured that the sensitivities of both microphones' channels were properly aligned at the 1 kHz calibration check frequency.

All test signals were carefully generated and conditioned to meet the requirements of the standardized test procedures [20], ensuring a reliable comparison with the mic_{ref}.

For the short-duration signal tests, tone bursts at 4 kHz with durations of 0.25 ms, 2 ms, and 200 ms were generated and played through the loudspeaker inside the anechoic test box. These bursts were created by temporally gating a continuous 4 kHz sinusoidal waveform. The signal amplitude was carefully adjusted to achieve a SPL of approximately 107 dB at the position of the mic_{ref}, a value selected to safely stay below the acoustic overload point (AOP) of microphones, and to remain about 3 dB below the maximum input limit of both analyzer channels to avoid signal clipping or distortion.

Linearity tests involved sending continuous 8 kHz sinusoidal signals to the loudspeaker with stepwise amplitude variations covering the dynamic range of the mic_{test}. The initial amplitude was set to yield a reference SPL of approximately 94 dB at the mic_{ref}. Background noise was accounted for under controlled laboratory conditions:

1) Noise corrections were applied when the difference between the total SPL and background noise fell between 3 dB and 10 dB.
2) For differences below 3 dB, the corrections were deemed unreliable, and the corresponding SPL marked the lower limit of the linearity test.
3) When the difference exceeded 10 dB, the influence of background noise was considered negligible, and no correction was applied.

B. Results of the Experiments

1) *Tone-Burst Response Analysis:* Standardized acoustic tone bursts at 4 kHz were used as excitation signals, providing controlled transient conditions that are ideal for evaluating the dynamic behavior of SLMs in accordance with IEC 61672-3 [20]. This approach enables a robust characterization of the MEMS microphone's temporal response. However, accurate loudspeaker reproduction is critical, especially for shorter bursts of 0.25 and 2 ms as loudspeaker limitations can significantly impact the signal integrity.
Residual tone-burst levels, R_{tb}, are defined in (6) as the difference between the sound pressure level measured during the tone burst, L_{m}, and the corresponding level, L, of the continuous signals in dB relative to 20 μPa. Measurements were carried out using three standard metrics for L_{m} determination: the maximum sound level with fast and slow time weighting, $L_{\text{Fast,max}}$ and $L_{\text{Slow,max}}$, respectively, and the A-weighted sound exposure level L_{AE} [8].

$$R_{\text{tb}} = L_{\text{m}} - L. \tag{6}$$

These residuals, calculated from both the mic_{test} and the mic_{ref}, were compared to the theoretical reference values provided by IEC 61672-1 [8]. Because the loudspeaker introduces systematic deviations due to its limited transient response, the difference between the residuals, ΔR_{tb}, was computed to isolate the performance of the MEMS microphone, as follows:

$$\Delta R_{\text{tb}} = R_{\text{tb,mems}} - R_{\text{tb,ref}}. \tag{7}$$

Table III summarizes the measured residuals and their differences across various burst durations and evaluation metrics.

TABLE III

MEASURED VALUES OF THE RESIDUAL TONE-BURST LEVELS, $R_{TB,REF}$ AND $R_{TB,MEMS}$, FOR THE MIC_{REF} AND THE $MIC_{TEST,MEMS}$, RESPECTIVELY, ALONG WITH THEIR DIFFERENCE, ΔR_{TB}, OBTAINED FOR THE 4 kHz TONE-BURST DURATIONS AND EVALUATION METRICS RECOMMENDED BY THE IEC 61672-3 STANDARD

Burst duration	Metrics	$R_{tb,ref}$ (dB)	$R_{tb,mems}$ (dB)	ΔR_{tb} (dB)
200 ms	$L_{Fast,max}$	-0.99	-1.05	-0.06
	$L_{Slow,max}$	-7.46	-7.45	0.01
	L_{AE}	-7.07	-7.06	0.01
2 ms	$L_{Fast,max}$	-17.17	-17.15	0.02
	$L_{Slow,max}$	-26.15	-26.14	0.01
	L_{AE}	-26.19	-26.19	0.00
0.25 ms	$L_{Fast,max}$	-25.22	-25.22	0.00
	L_{AE}	-34.24	-34.26	-0.02

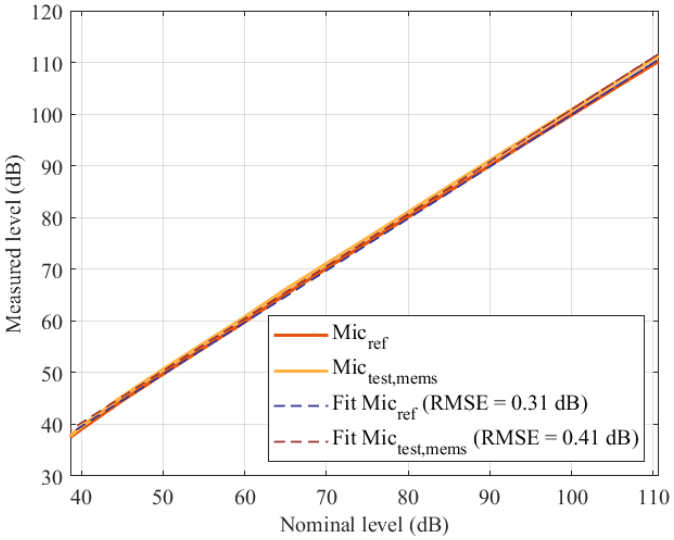

Fig. 12. Linearity assessment of mic_{ref} and $mic_{test,mems}$ after background noise correction, with linear regression fits and RMSE values across the dynamic range.

The following relative percentage errors were observed in the reference microphone residuals $R_{tb,ref}$, compared to IEC 61672-1 theoretical values as follows.

a) For 200 ms bursts: within ±1.5 %.
b) For 2 ms bursts: between −3.0 % and −4.6 %.
c) For 0.25 ms bursts: between −4.9 % and −6.6 %.

These errors are primarily attributed to the loudspeaker's transfer function, which introduces attenuation and distortion, particularly for shorter durations. The increasing deviation of the reference microphone residuals with decreasing burst duration provides a quantitative estimate of the loudspeaker transient response limitation, which is effectively canceled in the differential analysis between reference and MEMS microphones. The low values of ΔR_{tb} confirm that the digital MEMS microphone accurately detects short-duration acoustic events and preserves signal characteristics after the analog-to-digital conversion.

2) *Linearity Response Analysis*: A continuous 8 kHz sinusoidal tone was used to drive the loudspeaker, and its amplitude was varied in discrete steps across the expected dynamic range of the mic_{test}. The initial level was set to produce approximately 94 dB at the mic_{ref}. The system's linearity was evaluated by comparing the measured sound pressure levels, L, with the nominal values. Fig. 12 illustrates these measurements, including linear regression fits for both microphones. The regression analysis yields an RMSE of 0.31 dB for the mic_{ref} and 0.41 dB for the mic_{test}.

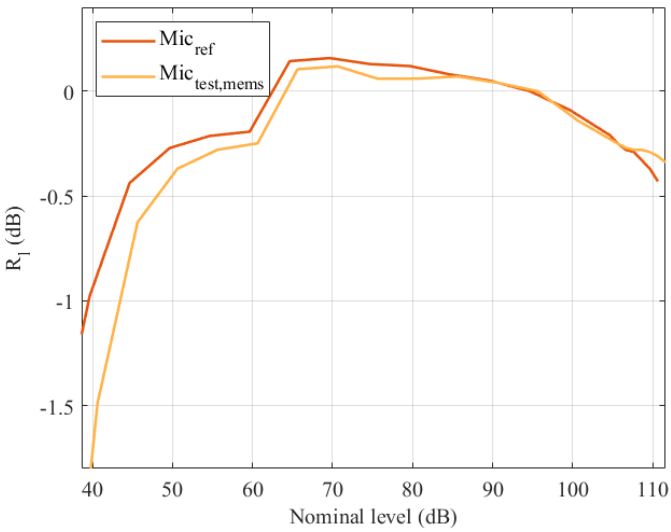

Fig. 13. Measured residual linearity levels, R_l, for the mic_{ref}, and $mic_{test,mems}$, microphones. These residuals highlight amplitude-dependent effects arising from both the loudspeaker and sensor responses.

The background noise effects were mitigated as follows.

a) The overall ambient noise level in the anechoic test box was measured as L_{noise} = 36.8 dB using the mic_{ref}.
b) Corrected level values, L', were obtained using (8) and were applied only when the difference, $L - L_{noise}$, fell between 3 dB and 10 dB [19].

$$L' = 10\log_{10}\left(10^{L/10} - 10^{L_{noise}/10}\right). \tag{8}$$

The residual linearity levels, R_l, were then calculated as follows [8]:

$$R_l = L' - L_{nom} \tag{9}$$

where L_{nom} corresponds to the nominal levels based on the initial calibration step. Fig. 13 shows the residuals, R_l, for both microphones. A clear amplitude-dependent trend is observed, mainly due to the loudspeaker's nonlinear behavior. Between 40 dB and 50 dB, where the SPL is closer to the noise floor (36.8 dB), the mic_{test} exhibits a slightly greater negative deviation, likely due to its sharper sensitivity curve compared to mic_{ref}, which is particularly peaked around 8 kHz. The observed amplitude-dependent trend in the residual linearity levels elucidates the RMSE values derived from the regression analysis of the linearity responses for both microphones.

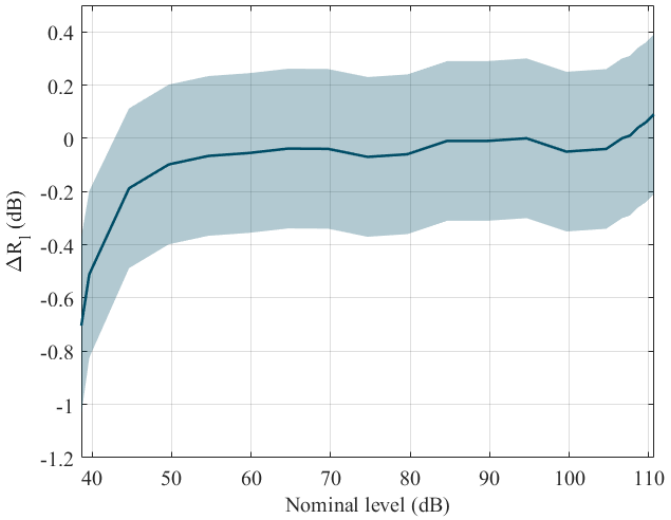

Fig. 14. Difference between the measured residual linearity levels, ΔR_l, plotted along with the associated measurement uncertainty. The measured values of ΔR_l quantify the $\text{mic}_{\text{test,mems}}$ performance independently of the loudspeaker behavior.

To decouple the microphone's linearity from that of the loudspeaker, the difference between the residuals of the two microphones was calculated as

$$\Delta R_l = R_{l,\text{mems}} - R_{l,\text{ref}}. \tag{10}$$

Fig. 14 shows the results of the deviation ΔR_l, plotted as a function of the nominal level. This provides a direct evaluation of the MEMS microphone's linearity, independent of artifacts induced by the loudspeaker. The results demonstrate consistent behavior across the tested range, with deviations remaining well within acceptable limits. The associated uncertainty is estimated to remain below 0.35 dB throughout the microphone's effective linear operating range from 38 dB to 110 dB, confirming the device's reliable performance for precision acoustic measurements.

C. Experimental Validation in Traffic Noise Scenarios

A set of controlled and repeatable laboratory experiments was conducted using representative traffic noise signals to evaluate the real-world performance of the digital MEMS microphone. Three 30-second audio sequences were selected from a recording dataset to test the mic_{test} under realistic sound spectral and temporal characteristics. These included: 1) conventional vehicle traffic noise; 2) motorway construction machinery (specifically, leveling equipment); and 3) two-stroke petrol engine operation.

The sequences were played back through the loudspeaker of the anechoic test box, which was driven by a Keysight 33500B function generator [36], loaded with the corresponding waveforms. A sampling rate of 20 kHz was selected to balance temporal resolution and data storage while preserving the spectral content up to 10 kHz. This ensured sufficient frequency fidelity for sensor characterization using third-octave band analysis [22].

Prior to playback, the signal amplitudes were adjusted via an audio amplifier. This ensured that the resulting SPLs exceeded the background noise level by at least 10 dB in every third-octave band from 100 Hz to 10 kHz.

Fig. 15 shows the three spectrograms corresponding to the different traffic noise sources. In the case of conventional vehicle traffic, Fig. 15(a), the energy is mainly distributed across low and medium frequencies, with occasional short-duration tonal sound components above 5 kHz. The spectrogram of leveling machinery in Fig. 15(b) shows a dominant of low frequencies, with a notable concentration around 160 Hz. The spectrogram of two-stroke engine noise Fig. 15(c), shows energy extending from approximately 200 Hz to 5 kHz, with marked temporal fluctuations and intermittent high-energy peaks associated with engine operation and mechanical components. Higher-intensity peaks predominantly occur between 400 Hz and 3 kHz, highlighting the relevance of the mid-frequency range in capturing such events.

Both the mic_{test} and the mic_{ref} were exposed to each signal simultaneously inside the anechoic test box. Equivalent continuous sound pressure levels L_{eq}, were measured across third-octave bands ranging from 100 Hz to 10 kHz. The spectrum analyzer operated in frequency analysis mode, and the raw measurements were corrected using the sensitivity values of the mic_{test} and the mic_{ref}, at the exact mid-frequencies of the third-octave bands, to account for their respective responses.

Fig. 16 shows the equivalent continuous sound pressure level L_{eq} across third-octave bands for the three traffic noise scenarios as measured by the mic_{ref}. Distinct spectral profiles can be observed for each noise source.

The conventional vehicle traffic signal (dark green) exhibits a broadband distribution, reaching a maximum L_{eq} of ~ 89.5 dB at 160 Hz, followed by a gradual decay in energy across higher frequency bands. This pattern reflects the composite nature of traffic noise, which usually consists of tire-road interactions, engine combustion, and aerodynamic components.

The noise generated by motorway construction leveling machinery (light green) exhibits a dominant low-frequency component, with a maximum L_{eq} of 92.9 dB at 125 Hz. This is characteristic of heavy machinery operation, wherein mechanical impacts, vibrations, and transmitted loads generate high-intensity acoustic emissions concentrated in the lower frequency range.

The two-stroke petrol engine signal (medium green) displays a spectral peak of 84.6 dB at 200 Hz, with notable energy content extending into the mid-frequency range up to approximately 5 kHz. This behavior corresponds to the cyclic combustion events and mechanical coupling, which are typical of small engine operation and are often accompanied by harmonics and high temporal variability.

Across all scenarios, a progressive attenuation is observed above 1 kHz, with spectral levels generally falling below 60 dB beyond 6.3 kHz, reflecting the limited high-frequency content of typical traffic noise sources.

To evaluate the MEMS microphone's spectral accuracy under these conditions, we analyzed the deviations between the L_{eq} values measured by the mic_{test} and the mic_{ref} across the

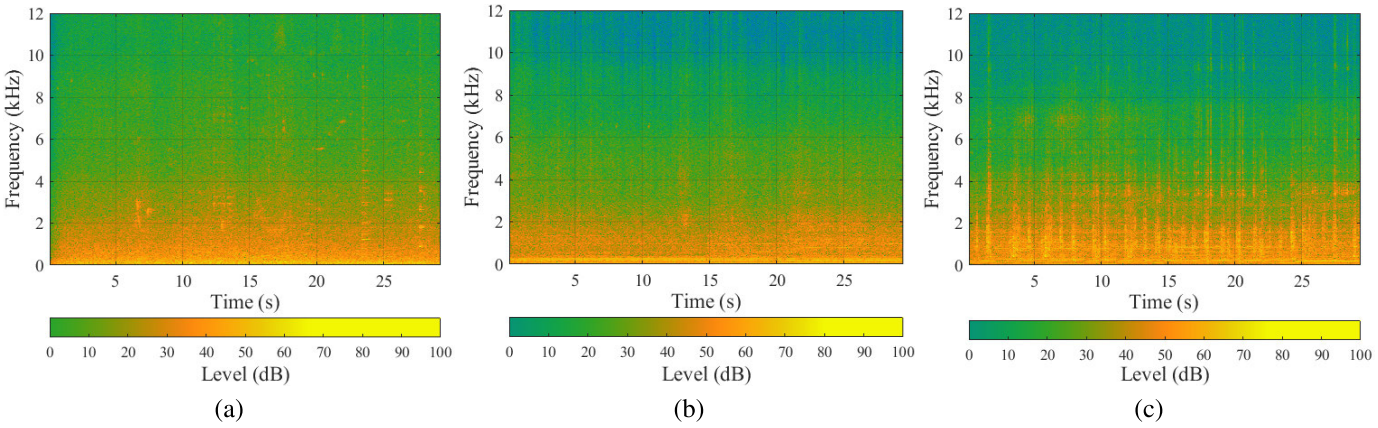

Fig. 15. Spectrograms of the representative traffic noise signals used in the experimental validation. (a) Conventional vehicle traffic. (b) Motorway construction leveling machines operation. (c) Two-stroke petrol engine operation.

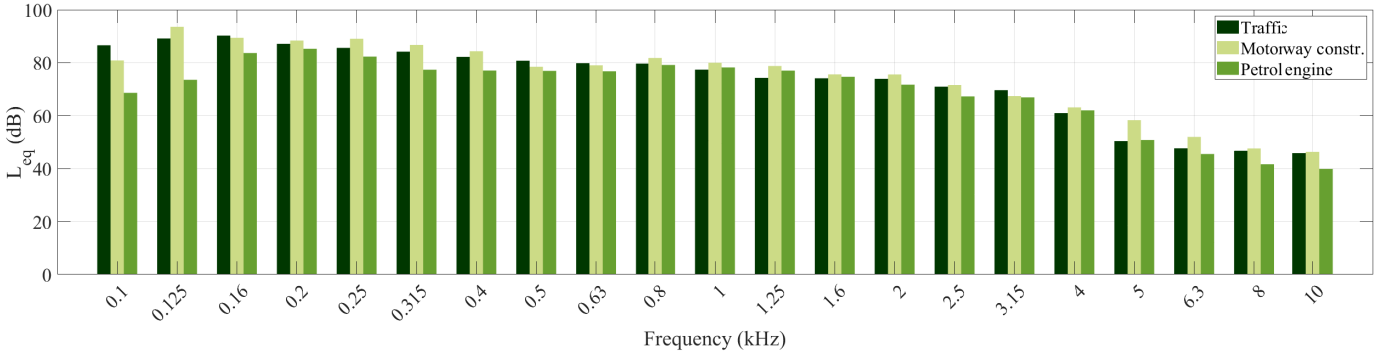

Fig. 16. Third-octave band frequency spectra of the three traffic noise scenarios, measured by the mic_{ref}.

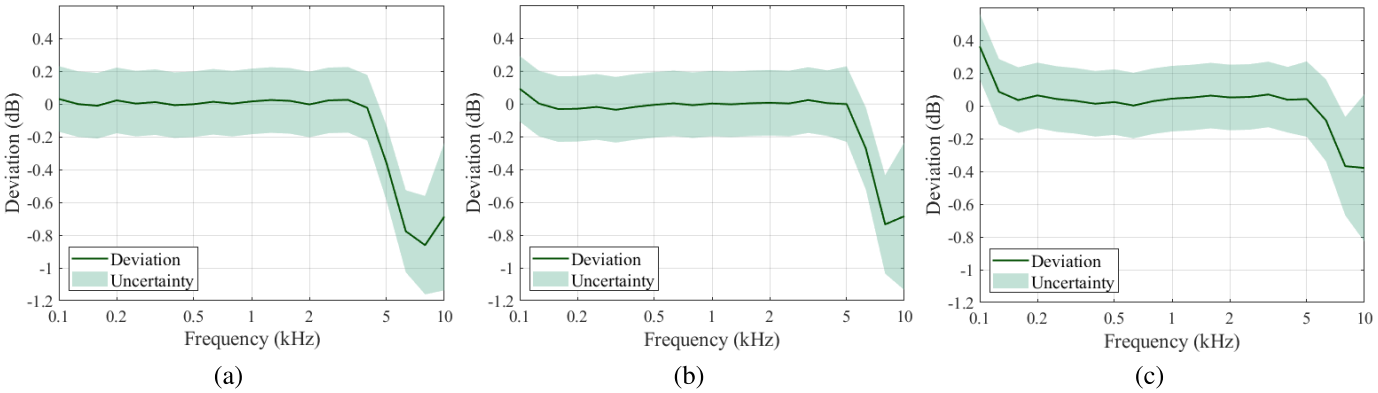

Fig. 17. Deviation between the L_{eq} measurements, provided by the $\text{mic}_{\text{test,mems}}$ and the mic_{ref} at the third-octave band frequencies, plotted with the associated measurement uncertainty, for the three traffic noise scenarios. (a) Conventional vehicle traffic noise. (b) Motorway construction leveling machines operation. (c) Two-stroke petrol engine operation.

relevant third-octave bands. The results, presented in Fig. 17, include the associated measurement uncertainties for each scenario.

A consistent pattern of increasingly large negative deviations is observed above 4 kHz in all cases. These deviations occur alongside the decreasing energy content of sound in the high-frequency range, with L_{eq} values decreasing from 60 to 40 dB, due to the nonflat sensitivity curve of the mic_{test}. Conversely, in the two-stroke engine scenario, a slightly increasing positive deviation is observed below 125 Hz, likely due to the low-frequency roll-off in the MEMS microphone's sensitivity curve.

The nonflat frequency response curve of the mic_{test} acts like a filter, introducing band-averaging errors and providing an inaccurate representation of the sound's spectrum. To avoid this issue, an inverse filter that compensates for the microphone's frequency response can be embedded in the microcontroller [11].

Measurement uncertainty increases with frequency, primarily due to the computational estimation of sound field

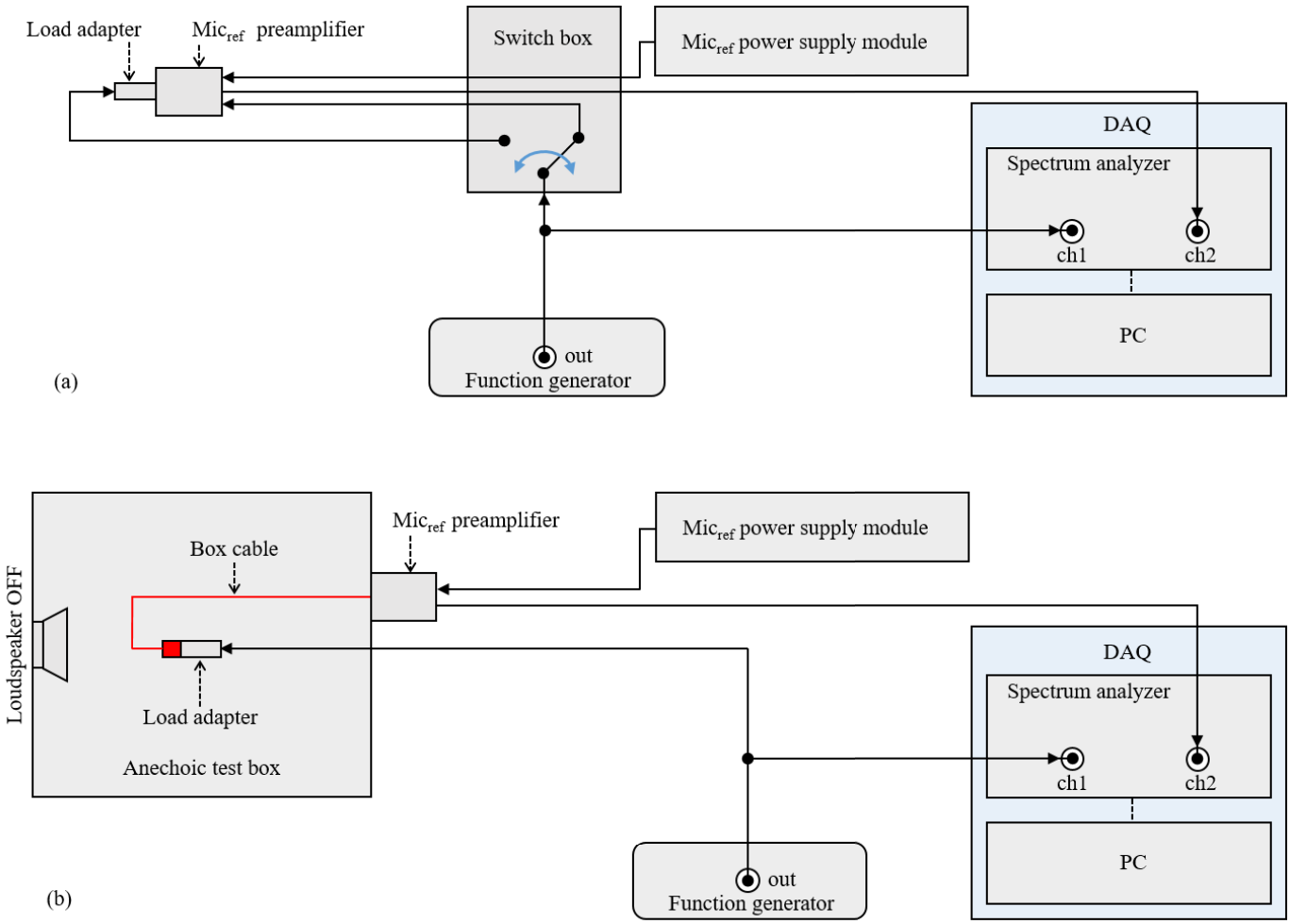

Fig. 18. Block diagram of the experimental setup used for the electrical characterization of the external gain of the mic$_{ref}$ measurement chain. (a) Setup for the determination of the gains of insert voltage preamplifier and load adapter, excluding the extension cable of the anechoic test box. (b) Setup for the determination of the overall gain including the extension cable of the anechoic test box.

correction factors. This contribution becomes significant above 4 kHz, reaching up to 0.45 dB at 10 kHz.

Overall, these results confirm that the digital MEMS microphone can reliably capture realistic traffic noise profiles in the range from 100 Hz to 5 kHz, validating its use in dynamic acoustic environments under controlled test conditions. However, a correction filter based on the MEMS microphone's sensitivity curve is expected to significantly improve the spectral representation of sounds, even in the low- and high-frequency ranges.

VI. Conclusion

This work presented a full-acoustic verification methodology for digital MEMS microphones in the context of traffic noise monitoring applications. The methodology uses a modular, traceable measurement architecture to characterize MEMS sensors under controlled laboratory conditions. Using standardized tones and representative traffic noise signals emitted inside an anechoic test box, the proposed approach allows one to compare the response of a digital MEMS microphone to that of a reference Laboratory Standard microphone simultaneously exposed to the same signal.

The results demonstrate that, when properly calibrated, digital MEMS microphones can achieve measurement performance comparable to that of conventional reference instruments, while offering advantages in terms of cost, portability, and scalability. This methodology provides a repeatable and traceable solution for fully evaluating the response of digital MEMS microphones, thereby bridging the gap between innovation and adherence to international metrological standards. Furthermore, it enables the verification of MEMS-based instrumentation for sound level metering using a full-acoustic approach, which overcomes issues related to developing electronic circuits that substitute MEMS microphones for electrical signal testing.

Although the experimental validation is demonstrated using a specific digital MEMS microphone model, the proposed full-acoustic verification methodology is inherently applicable to a wide range of digital MEMS microphones, as it does not depend on microphone-specific electrical interfaces or internal architectures.

The main contribution of this work lies in the definition of a full-acoustic, SI-traceable verification methodology tailored to the digital architecture of MEMS microphones, which inherently precludes the application of conventional electrical

TABLE IV
DESCRIPTION OF THE INSTRUMENTATION USED IN THE EXPERIMENTAL SETUP

Instrument	Model	Description
Anechoic test box	Brüel & Kjær Type 4232	Ensures high-fidelity signal reproduction and external noise isolation (100 Hz–10 kHz).
Digital MEMS microphone (mic_{test})	Knowles SPH0645LM4H-B with Adafruit I^2S	Low-noise capture, direct digital interface.
Microcontroller	Teensy® 4.1	ARM Cortex-M7, 600 MHz, for advanced audio and embedded processing.
DAC	PCM5102A – Texas Instruments	Digital-to-analog converter typically used with boards such as the Teensy 4.1 for audio applications.
Reference microphone (mic_{ref})	Brüel & Kjær Type 4180	High-precision 1/2" Laboratory Standard (LS2) condenser microphone. Frequency range up to 20 kHz.
Spectrum analyzer	Ono Sokki DS-3200	Multichannel FFT analyzer with dual-channel 100 kHz Range Input Unit DS-0366.
Microphone preamplifier	Brüel & Kjær Type 2673	High-precision insert voltage preamplifier, 3 Hz – 200 kHz bandwidth.
Waveform generator	Keysight 33500B	Predefined or arbitrary waveform generator, sampled and loaded into the instrument's memory via USB port. 16-bit resolution, 1 mVpp–10 Vpp output.

TABLE V
ESTIMATED CONTRIBUTIONS OF THE MAIN UNCERTAINTY SOURCES CONSIDERED FOR THE CHARACTERIZATION OF THE MEMS MICROPHONE RESPONSE

Uncertainty Source	Contribution (dB)
Calibration of reference microphone sensitivity	0.05 – 0.08
Measurement of total external gain	$\sim$ 0.10
DAC's frequency response and linearity	$\sim$ 0.15
Numerical estimation of sound-field corrections ($>$ 4 kHz)	0.10 – 0.40
Microphone positioning inside the anechoic test box	$<$ 0.10
Background noise fluctuations (SPL 38–45 dB)	0.10 – 0.30
Data acquisition system limitations (linearity, resolution, transient response)	$\sim$ 0.15
Measurement repeatability (based on five repetitions)	$\sim$ 0.10

substitution tests. By combining standardized acoustic test signals, realistic traffic noise scenarios, and sound-field corrections derived from numerical simulations, the proposed framework provides a robust and repeatable approach for assessing the suitability of digital MEMS microphones for sound level metering applications. This work bridges the gap between low-cost sensor technologies and metrological requirements, supporting the deployment of dense and reliable acoustic sensor networks for traffic noise monitoring.

APPENDIX A

Table IV shows the measurement instruments and devices employed for the experimental characterization and evaluation tests.

APPENDIX B

Fig. 18(a) presents the block diagram of the experimental setup used to characterize the electrical gain of the load adapter and the insert voltage preamplifier of the reference microphone, excluding the extension cable of the anechoic test box. A switch box allows the selection between two input paths. Sinusoidal test signals with a constant amplitude of 12.5 mV_{rms}, spanning the frequency range from 100 Hz to 10 kHz at third-octave center frequencies, are supplied by a signal generator.

The signals can be routed either as follows.

1) To the load adapter input, enabling the measurement of the combined gain of the load adapter and the insert voltage preamplifier, or
2) To the insert voltage preamplifier input, to isolate and evaluate only the gain of the preamplifier.

Fig. 18b illustrates the configuration used to evaluate the overall electrical gain of the mic_{ref} measurement chain, including the load adapter, the extension cable of the anechoic test box, and the insert voltage preamplifier.

Since the extension cable cannot be disconnected, the test is conducted inside the anechoic test box with the loudspeaker off. The same sinusoidal test signals (12.5 mV_{rms}, spanning from 100 Hz to 10 kHz at third-octave center frequencies) are directly applied to the input of the load adapter.

APPENDIX C

The main sources of uncertainty affecting the characterization of the MEMS microphone response were identified and quantified based on the experimental procedures described throughout the study. These include the calibration of reference instrumentation, signal processing limitations, environmental conditions, and setup-related factors. Table V summarizes the estimated contributions of each component.

REFERENCES

[1] J. Hong, J. Kim, C. Lim, K. Kim, and S. Lee, "The effects of long-term exposure to railway and road traffic noise on subjective sleep disturbance," *J. Acoust. Soc. Amer.*, vol. 128, no. 5, pp. 2829–2835, Nov. 2010.

[2] J. L. Eberhardt, L.-O. Straale, and M. H. Berlin, "The influence of continuous and intermittent traffic noise on sleep," *J. Sound Vib.*, vol. 116, no. 3, pp. 445–464, Aug. 1987.

[3] M. Basner et al., "Auditory and non-auditory effects of noise on health," *Lancet*, vol. 383, no. 9925, pp. 1325–1332, Apr. 2014.

[4] D. Michaud, M. Guay, S. Keith, A. Denning, and J. Mcnamee, "A preliminary analysis of long-term self-reported sleep disturbance attributed to wind turbines and modelled outdoor nightly average wind turbine sound pressure level," in *Proc. INTER-NOISE NOISE-CON Congr. Conf.*, vol. 270, no. 11, pp. 387–400, Oct. 2024.

[5] W. Yang, J. He, C. He, and M. Cai, "Evaluation of urban traffic noise pollution based on noise maps," *Transp. Res. D, Transp. Environ.*, vol. 87, Oct. 2020, Art. no. 102516.

[6] J. Peng, J. Parnell, and N. Kessissoglou, "Spatially differentiated profiles for road traffic noise pollution across a state road network," *Appl. Acoust.*, vol. 172, Jan. 2021, Art. no. 107641.

[7] A. Can et al., "The future of urban sound environments: Impacting mobility trends and insights for noise assessment and mitigation," *Appl. Acoust.*, vol. 170, Dec. 2020, Art. no. 107518.

[8] Electroacoustics-Sound Level Meters-Part 1: Specifications, Standard IEC 61672-1:2013, International Electrotechnical Commission, Geneva, Switzerland, 2013.

[9] C. Mydlarz, J. Salamon, and J. P. Bello, "The implementation of low-cost urban acoustic monitoring devices," *Appl. Acoust.*, vol. 117, pp. 207–218, Feb. 2017.

[10] P. Guidorzi and M. Garai, "A low-cost system for quick measurements on noise barriers in situ," *IEEE Trans. Instrum. Meas.*, vol. 71, pp. 1–14, 2022.

[11] F. R. D. Mello and W. D. Fonseca, "Autonomous noise monitoring system based on digital MEMS microphones: Development of a smartphone application for remote communication," in *Proc. INTER-NOISE NOISE-CON Congr. Conf.*, Feb. 2023, vol. 265, no. 2, pp. 5650–5661.

[12] Q. Wang, Y. Zhang, S. Cheng, X. Wang, S. Wu, and X. Liu, "MEMS acoustic sensors: Charting the path from research to real-world applications," *Micromachines*, vol. 16, no. 1, p. 43, Dec. 2024.

[13] F. R. D. Mello, W. D. Fonseca, and P. H. Mareze, "MEMS digital microphone and Arduino compatible microcontroller: An embedded system for noise monitoring," in *Proc. INTER-NOISE NOISE-CON Congr. Conf.*, 2021, vol. 263, no. 3, pp. 3921–3932.

[14] J. Picaut, A. Can, N. Fortin, J. Ardouin, and M. Lagrange, "Low-cost sensors for urban noise monitoring networks—A literature review," *Sensors*, vol. 20, no. 8, p. 2256, Apr. 2020.

[15] T. Koukoulas et al., "Cross-comparison of the optical and acoustical calibration methods for microphones based on microelectromechanical system technologies," in *Proc. INTER-NOISE NOISE-CON Congr. Conf.*, 2024, vol. 270, no. 5, pp. 6049–6060.

[16] M. Chan, C. Baker, D. Simmons, and M. Goldsmith, "Bulk calibration method of micro-electromechanical system (MEMS) microphones," *J. Acoust. Soc. Amer.*, vol. 150, no. 2, pp. 1402–1410, Aug. 2021.

[17] D. Hermawanto, K. Ishikawa, K. Yatabe, and Y. Oikawa, "Determination of frequency response of MEMS microphone from sound field measurements using optical phase-shifting interferometry method," *Appl. Acoust.*, vol. 170, Dec. 2020, Art. no. 107523.

[18] W.-H. Cho and T. Koukoulas, "Signal processing considerations on the optical measurement of acoustic particle velocities in free-field conditions," *IEEE Trans. Instrum. Meas.*, vol. 69, no. 7, pp. 4021–4032, Jul. 2020.

[19] A. Prato, N. Montali, C. Guglielmone, and A. Schiavi, "Pressure calibration of a digital microelectromechanical system microphone by comparison," *J. Acoust. Soc. Amer.*, vol. 144, no. 4, pp. EL297–EL303, Oct. 2018.

[20] Electroacoustics-sound Level Meters—Part 3: Periodic Tests, Standard IEC 61672-3:2013., International Electrotechnical Commission, Geneva, Switzerland, 2013.

[21] A. Gemelli et al., "Recent trends in structures and interfaces of MEMS transducers for audio applications: A review," *Micromachines*, vol. 14, no. 4, p. 847, Apr. 2023.

[22] L. L. Beranek and T. J. Mellow, *Acoustics: Sound Fields and Transducers*, 2nd ed. Academic Press, 2019.

[23] F. Saba, M. Campo-Valera, D. Paesante, G. Durando, M. Corallo, and D. Pugliese, "Effectiveness of sound field corrections for high-frequency pressure comparison calibration of MEMS microphones," *Sensors*, vol. 25, no. 5, p. 1312, Feb. 2025.

[24] (2021). *Brüel & Kjær Anechoic Test Box Type 4232*. [Online]. Available: https://www.bksv.com/-/media/literature/Product-Data/bp1668.ashx

[25] *Adafruit I2S MEMS Microphone Breakout-SPH0645LM4H*. Accessed: Jul. 15, 2025. [Online]. Available: https://learn.adafruit.com/adafruit-i2s-mems-microphone-breakout

[26] D. Pecioski, S. D. Markovska, V. Gavriloski, M. Anachkova, and A. I. Angjusheva, "Development of low-cost MEMS microphone array for sound localization in urban environments," in *Proc. INTER-NOISE NOISE-CON Congr. Conf.*, 2024, vol. 270, no. 7, pp. 4641–4651.

[27] PJRC.(2020). *Teensy 4.1 Technical Specifications*. [Online]. Available: https://www.pjrc.com/store/teensy41.html

[28] *Digital Analog Conversor DAC, PCM5102A*. Accessed: Jul. 15, 2025. [Online]. Available: https://www.ti.com/product/es-mx/PCM5102A

[29] (2019). *Brüel & Kjær Laboratory Standard Microphone Cartridge Types 4160 and 4180*. [Online]. Available: https://www.bksv.com/media/doc/bp0459.pdf

[30] Measurement Microphones—Part 1: Specifications for Laboratory Standard Microphones, Standard IEC 61094-1:2000, International Electrotechnical Commission, Geneva, Switzerland, 2000.

[31] *DS-3200 Multi-Channel Data Station–Ono Sokki*. Accessed: Jul. 15, 2025. [Online]. Available: https://www.onosokki.co.jp/English/hp_e/products/keisoku/data/ds3000.html

[32] Electroacoustics-octave-band and Fractional-octave-band Filters-part 1: Specifications, Standard IEC 61260-1:2014, International Electrotechnical Commission, Geneva, Switzerland, 2014.

[33] *Brüel & Kjær Type 2673 1/2-Inch Microphone Preamplifier With Insert Voltage Facility*. [Online]. Available: https://www.bksv.com/es/transducers/acoustic/microphones/preamplifiers/2673

[34] R. Barham, S. Barrera-Figueroa, and J. E. M. Avison, "Secondary pressure calibration of measurement microphones," *Metrologia*, vol. 51, no. 3, pp. 129–138, Jun. 2014.

[35] Y. He, A. Yu, X. Liu, and Y. Wang, *Micro-Electro-Mechanical Systems (MEMS). In Handbook of Integrated Circuit Industry*. Cham, Switzerland: Springer, 2024, pp. 895–911.

[36] Keysight Technologies.(2018). *33500B Series Trueform Waveform Generators*. [Online]. Available: https://www.keysight.com/us/en/assets/7018-05928/data-sheets/5992-2572.pdf

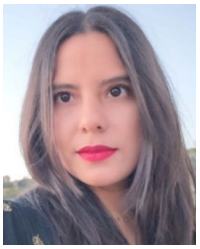

María Campo-Valera was born in Santa Marta, Colombia, in 1984. She received the B.Sc. degree in sound engineering from San Buenaventura University, Bogotá, Colombia, in 2009, the M.Sc. degree in acoustic engineering from the Universitat Politécnica de Valéncia (UPV), Valencia, Spain, in 2016, and the Ph.D. degree from the Universidad Politécnica de Cartagena (UPCT), Cartagena, Spain, in 2020.

In January 2021, she was a Post-Doctoral Researcher at UPCT. In January 2022, she joined at Universidad de Málaga, Málaga, Spain, as a Post-Doctoral Researcher awarded a competitive two-year grant, named Margarita Salas (fully funded by the European Commission). She was a Visiting Researcher at the Escuela Naval de Cadetes Almirante Padilla (ENAP), Cartagena de Indias, Colombia. She was an Assistant Professor at the Universidad de Málaga. She is currently an Associate Professor with the Universidad Internacional de la Rioja (UNIR), Logro ño, Spain. Her interests include signal processing, sensor design, finite element method (FEM), nonlinear acoustics, and underwater acoustic communications.

Fabio Saba was born in Italy in 1985. He received the M.Sc. degree in energetic and nuclear engineering and the Ph.D. degree in energetics from the Politecnico di Torino, Turin, Italy, in 2011 and 2017, respectively.

He is currently a Researcher with the Istituto Nazionale di Ricerca Metrologica (INRiM), Turin, where he is responsible of the Acoustic Sound-in-Air Laboratory. He is a Contact Person for the subcommittee SC-A (Sound in Air) of the European Technical Committee EURAMET TC-AUV (Acoustics, Ultrasounds and Vibration), and a member of the working group WG 5 (Measurement Microphones) of the Technical Committee of the International Electrotechnical Commission IEC TC 29 (Electroacoustics). His main research field and expertise include acoustic metrology and measurement science, flow metrology and thermal energy measurements, finite element method (FEM), and uncertainty analysis.

Mario Corallo was born in Italy in 1972.

He obtained a professional qualification as a Repair Technician for Electronic Equipment in July 1990. Since January 1998, he has been working as a Technical Operator at the Acoustics Sound-in-Air Laboratory, Istituto Nazionale di Ricerca Metrologica (INRiM), Turin, Italy. His activities include performing precise measurements of the acoustic properties of materials, calibrating instruments used to determine sound pressure levels, and supporting the development of metrological methodologies in the field of acoustics. Over the years, he has contributed to various laboratory projects aimed at ensuring traceability to the International System of Units.

Paolo Guidorzi was born in Italy in 1969. He received the M.Sc. degree in electrical engineering and the Ph.D. degree in applied acoustics from the University of Bologna, Bologna, Italy, in 1995 and 1999, respectively.

He is currently an Associate Professor with the Department of Industrial Engineering, School of Engineering, University of Bologna. His current research interests include noise barrier measurement, signal processing, development of hardware and software for acoustic measurement instruments, and acoustic measurements.

Andrea Osele was born in Italy in 1977.

He handles acoustic measurements and design with Autostrada del Brennero S.p.A., Trento, Italy, and serves as a Scientific Coordinator for acoustic research activities. His research focuses on improving the performance of noise barriers and studying the acoustic properties of sound-absorbing materials.

Carlo Costa was born in Italy in 1965. He received the M.Sc. degree in civil engineering in transportation systems from the University of Bologna, Bologna, Italy, in 1991.

He is the General Technical Director of Autostrada del Brennero S.p.A., Trento, Italy, a Vice President of Technical Committee 3.5 "Road Infrastructure for Road Transport Decarbonization" and a member of Technical Committee 3.2 "Winter Services" of the Italian National Committee of the World Road Association (PIARC), and a coordinator in charge of several European projects. More than 2,000 projects drafted in the field of construction or rehabilitation of civil works, roads, viaducts, tunnels, and technological systems, for a total amount of over 12 billion euros.